Food Control 133 (2022) 108588

Contents lists available at ScienceDirect

Food Control

journal homepage: www.elsevier.com/locate/foodcont

Rapid detection of adulteration in desiccated coconut powder: vis-NIR spectroscopy and chemometric approach

R. Pandiselvam [a,*], Naveen Kumar Mahanti [b,d,**], M.R. Manikantan [a,***], Anjineyulu Kothakota [c], Subir Kumar Chakraborty [d], S.V. Ramesh [a], P.P. Shameena Beegum [a]

[a] Physiology, Biochemistry and Post-Harvest Technology Division, ICAR-Central Plantation Crops Research Institute, Kasaragod, 671 124, Kerala, India
[b] College of Horticulture-Chinalataripi, Dr. Y.S.R Horticultural University, West Godavari, Andhra Pradesh, India
[c] Agro-Processing & Technology Division, CSIR-National Institute for Interdisciplinary Science and Technology (NIIST), Trivandrum, 695 019, Kerala, India
[d] Agro Produce Processing Division, ICAR-Central Institute of Agricultural Engineering, Nabibagh, Berasia Road, Bhopal, MP, 462038, India

ARTICLE INFO

Keywords:
Coconut milk residue
Fat
Virgin coconut oil
Selected wavelengths
PLSR
PLS-DA
PCA

ABSTRACT

Adulteration of desiccated coconut powder (DCP) with coconut milk residue (CMR) is an emerging problem in the coconut processing industry. Consumers and industries are looking for a simple non-destructive device to measure the purity of DCP. vis-NIR (350–2500 nm) spectroscopy along with the chemometric techniques have been used to assess the purity of DCP. In this study, DCP was adulterated with CMR at different levels such as 0 (pure DCP), 10, 20, 30, 40, 50, 60, 70, 80, 90, and 100% (pure CMR). Partial least squares regression (PLSR) models were developed using whole spectral data and selected wavelengths. The spectral data were pre-processed using different techniques such as raw, MSC + SNV, SG-smoothing, and detrending. The R^2 of the models constructed with the pre-processed spectral data was higher than 0.950, irrespective of pre-processing technique. Pre-processing of spectral data does not have a significant effect on model performance when compared with the model developed using raw spectral data ($R^2_P = 0.973$; $SE_P = 9.681$; $RPD_P = 9.381$; $RER_P = 10.389$), but the prediction accuracy was decreased. The wavelengths 653, 933, 1189, 1383, 1444, 1670, and 1911 nm were selected as the featured wavelengths for quantification of adulteration level in DCP. No significant difference in statistical results was observed between the PLSR model developed with selected wavelengths ($R^2_P = 0.869$; $SE_P = 11.701$; $RPD_P = 9.381$; $RER_P = 8.595$) and the PLSR model for whole spectral data. The developed model can be used to predict the level of adulteration in DCP if the adulterant concentration was more than 10%. The overall results obtained in present study suggest that the vis-NIR spectroscopy along with suitable chemometric techniques have a great potential for rapid measurement of adulteration level in DCP.

1. Introduction

Desiccated coconut powder (DCP) is an important value added product obtained from coconut meat or kernel. It has been widely used in food applications of confectionery, puddings, and bakery industries. Also, it serves as a substitute for fresh coconut gratings for the preparation of various food items. DCP processing involves selection of properly matured nuts (11–12 months), removal of exocarp and mesocarp (husk) layer, deshelling, paring (testa removal), blanching, pulverizing, drying, and packaging (Manikantan et al., 2018). Several types of machinery such as mechanical dehusking machine, deshelling machine, testa removing machine, disintegrator (or shredding), dryer (fluidized bed dryer), and packaging machine are employed in the processing of DCP. The final moisture content of DCP is adjusted to 2.5–3.0% (w.b.) in the drying process.

Biochemical characterization of DCP revealed that it has healthy fats and dietary fibers. As per the regulations of Food Safety and Standards Authority of India (2011), the DCP should have at least 55% oil content and a maximum of 3% moisture and 2.5% ash. Also, it contains 18–20% carbohydrate, 6.0–6.6% protein, and 4–6% crude fibre (Coconut Development Board, 2017; Manikantan et al., 2018). The nutritional composition of DCP shows that it is rich in healthy saturated fats and a

* Corresponding author.
** Corresponding author. College of Horticulture-Chinalataripi, Dr. Y.S.R Horticultural University, West Godavari, Andhra Pradesh, India.
*** Corresponding author.
E-mail addresses: anbupandi1989@yahoo.co.in (R. Pandiselvam), naveeniitkgp13@gmail.com (N.K. Mahanti), manicpcri@gmail.com (M.R. Manikantan).

https://doi.org/10.1016/j.foodcont.2021.108588
Received 3 July 2021; Received in revised form 23 September 2021; Accepted 29 September 2021
Available online 30 September 2021

good source of dietary fiber. The medium chain fatty acids (especially lauric acid) present in coconut meat has antiviral, antibacterial, and antiprotozoal properties (DebMandal & Mandal, 2011; Manikantan et al., 2018; Pandiselvam et al., 2019; Trinidad et al., 2006). Recently published reports confirm that coconut fat in human diet improves immune system of the body and protects the liver against alcohol damage (Coconut Development Board, 2017). The carbohydrates of DCP are composed of cellulose, hemicellulose, glucose, mannose, and manno-oligosaccharides (Khuwijitjaru et al., 2012). Numerous studies have revealed that the consumption of fiber-rich foods could reduce the problems associated with heart diseases such as high blood pressure, diabetes, and high cholesterol, and colon cancer (Kaczmarczyk et al., 2012; Park et al., 2011; Trinidad et al., 2006).

However, the health benefits of DCP have been negated by the addition of coconut milk residue (CMR). CMR is the by-product obtained from virgin coconut oil and coconut milk processing industries. It is a low value by-product produced during coconut milk extraction. DCP is the most popular coconut product in the international market. The world production rate of DCP is 0.6 million MT in 2017 (Sebastian, 2017). Philippines, India, Indonesia, and Sri Lanka are the major exporters of DCP. Larger importers of DCP are the USA, Singapore, Brazil, Turkey, and Germany. India is the largest consumer of DCP. The production capacity of all 150 DCP units located in India is about 0.1 million MT (Sebastian, 2017). However, the DCP is being adulterated with CMR due to its large demand in the domestic and international market and attractive price. No previous studies have reported the authentication and purity assessment of DCP. However, in the market no standard methodologies, protocols or technologies are available for authentication of DCP. The presence of CMR in DCP can be assessed by comparing chemical composition of the adulterated sample with that of standard DCP. This exercise requires valuable chemicals, sophisticated equipment, skilled manpower, and is also a time-consuming process. Therefore, there is a need for a rapid and reliable technique which could be used in-line/online analysis of a food process industry. Visible-Near Infrared (vis-NIR) spectroscopy is a promising technology extensively accepted by the food industries for food quality and safety control because it requires no sample preparation. This technique has the capability to study the chemical composition from a single spectrum, and is rapid in nature, and is amenable for in-line, at line, and on-line analysis. It has been successfully adopted for the authentication of various edible oils (Jiménez-Carvelo et al., 2019; Picouet et al., 2018), coffee powder (Correia et al., 2018; Giraudo et al., 2019), cereals (Shao et al., 2018; Su & Sun, 2017), and honey (Guelpa et al., 2017). Reports of the use of vis-NIR spectroscopy has been made with regard to the authentication of extra virgin coconut oil (Manaf et al., 2007; Mansor et al., 2011), however, there are no studies pertaining to the use of this technique in authentication of DCP. Hence, the present study was conducted to analyze the potential of vis-NIR spectroscopy on the adulteration detection in DCP. The objective was to develop multivariate models using whole spectral data; to check the effect of spectral pre-processing on model performance; to identify the specific wavelengths which are capable of detecting the level of adulteration and development of a robust model using these selected wavelengths.

2. Materials and methods

2.1. Sample preparation and data collection

Matured coconuts (12 months old; var. West Coast Tall [WCT]) were dehusked, deshelled, testa was removed and the coconut water was discarded and pulverized using the equipment developed in-house (Manikantan et al., 2018). The pulverized gratings were dried in the hot-air electrical dryer at 60 °C till it reaches the safe moisture content (<3%). The completely dried gratings were packed in LDPE pouches (200 μm) and marked as desiccated coconut powder (DCP). The adulterant, coconut milk residue (CMR), was collected during the extraction of coconut milk. The CMR was then dehydrated using a dryer at 60 °C until it reaches the moisture 2.5–3% (w.b). And then the sample was packed in LDPE pouches (200 μm) and stored under atmospheric conditions until further use. The particle size of both DCP and CMR were detected using the ASABE S319.3 method (ASABE, 2003) in a Ro-Tap sieve shaker. The mean particle size of DCP and CMR was 2.5 ± 0.5 mm and 2.3 ± 0.4 mm, respectively.

The DCP was mixed with CMR in different proportions such as 0 (pure DCP), 10, 20, 30, 40, 50, 60, 70, 80, 90, and 100% (w/w) (pure CMR). For each level of adulteration 20 samples were prepared, and hence a total of 220 (11 × 20) samples were prepared. The spectral reflectance values of these samples were recorded using an IR spectrophotometer (Field Spec® 3 ASD Inc., Malvern P analytical Ltd, Malvern, UK) within the range of 350–2500 nm by placing the samples in Petri plates (100 mm diameter × 15 mm height). Each sample has undergone the scanning process for 10 times at different positions and averaged to a single value.

2.2. Spectroradiometer system

Spectral data of coconut powder was acquired in reflectance mode using IR spectroradiometer (Field Spec® 3 ASD Inc., Malvern P analytical Ltd, Malvern, UK). The spectroradiometer contains three different holographic diffraction gratings along with three detectors. Each and every detector is enclosed within the filters in order to avoid the second and higher order light. vis-NIR (350–1000 nm) detector was made up of silicon photodiode array, short wave infrared-SWIR1 (1000–1830 nm) diode was made up of Indium gallium arsenide (InGaAs) and short wave infrared-SWIR2 (1830–2500 nm) was constructed with InGaAs photodiode. The field of view (FOV) of the sensor was held at 25° as fixed by the manufacturer. Prior to acquiring the spectral data of coconut powder, the spectroradiometer was calibrated by black and white (99% reflective teflon plate) references. The spectral data was acquired within the spectral range of 350–2500 nm in the presence of 50 W tungsten halogen lamps with 3 and 10 nm spectral resolution within 350–700 and 700–2500 nm spectral range, respectively. These lamps were positioned at angle 45° with respect to the sample. The spectral data of the all the samples were acquired with the help of RS^3 software. The performance of the instrument was examined for every 15 min following the protocols suggested by the manufacturer.

2.3. Preprocessing of spectral data

The acquired spectral data could have been influenced by the noise arising from light scattering, particle size variation, and instrumental drift. Hence, to determine the level of adulteration precisely, the raw spectral data was corrected by adopting pre-processing techniques. In the present study, the spectral data was pre-processed to avoid undesirable light scattering and spectral noise. The raw spectral data was corrected using some spectral pre-processing methods such as the combination of multi scatter correction (MSC) and standard normal variate (SNV), de-trending (DT), and Savitzky–Golay (SG)-Derivative treatment (Derivative order-1st; polynomial order-2; window size-5).

2.4. Principal component analysis (PCA)

PCA is a widely utilized multivariate analysis technique used to transform a large dataset into a smaller dimension in which there are several inter-correlated variables while retaining most of the information that the dataset aims to convey (Ravikanth et al., 2017). PCA is generally used for data dimension reduction, eliminate multicollinearity, and enhance the hyperspectral dataset to ease feature selection (Romero, 2010). Thus, PCA is a data compression technique based on the correlation among the variables. It depends on the revamp of original data set into appreciably smaller sets of uncorrelated variables known as principal components (PCs). These PCs retain the

maximum amount of information from the original data set (Tao et al., 2015; Mahanti & Chakraborty, 2020). During PCA analysis the independent data set (X) is disintegrated into scores (T) and loading (P) matrices, such that X = TP (Arjun et al., 2021). The score matrix (T) denotes position of the sample in a new coordinate system and the loading matrix (P) represents how the PCs are built from the old axes (Park et al., 2003). In this study, PCA is used for exploratory analysis.

2.5. Model development and evaluation

Partial least squares regression (PLSR) models were developed to correlate the spectral data of sample and their corresponding adulteration level. PLSR is an advanced technique that combines the features of principal component analysis (PCA) and regression (Mahanti et al., 2020). The main drawbacks of analyzing the spectral data, collinearity and overlapping of bands, were effectively adressed in this PLSR model. This technique is expedient, where the number of independent variables is higher than the number of dependent variables (Barbin et al., 2012; Iqbal et al., 2013). PLSR tries to maximize the covariance, thus capturing the variance and correlating the data together (Xiaobo et al., 2010). The basic principle behind the PLSR is to extract the latent variables (LVs) accounting for as much of the marked factor variation as possible while it models the responses (Roy et al., 2015).

The signal to noise ratio at the beginning (350–400 nm) and end (2400–2500 nm) of the spectrum were very low therefore these portions were excluded from the model construction. The PLSR model was constructed using Nonlinear Iterative Partial Least Squares (NIPALS) algorithm exploying the raw, pre-processed spectral data (400–2400 nm) and selected wavelengths by using Unscrambler X 10.4 software. The spectral data (of 220 samples) was divided into two sets in 60:40 ratios. The first 60% (132 samples) of data was used for model calibration (C) and the constructed model was internally cross-validated (CV) with five CV groups. The remaining 40% (88 samples) of data was used for prediction (P) of developed model. The best model was selected on the basis of the statistical results and the same model was used for the selection of significant variables (wavelengths). The featured wavelengths were chosen based on the regression coefficients, and the PLSR model was constructed with these selected wavelengths.

2.6. Assessment of statistical performance of models

The performance of developed multivariate models were assessed based on the statistical results obtained during model cross-validation (CV) such as coefficient of determination (R^2_{CV}), and standard error (SE_{CV}), bias, slope and residual predictive deviation (RPD_{CV}). The RPD was estimated to standardize the SE; it is the ratio between SD and SE (Chakraborty et al., 2021). If the RPD value of model is greater than the 2.5, the performance of model was considered excellent, if it is between 2.0 and 2.5 the performance of model was considered very good, if it is between 1.8 and 2.0 it signifies that the model was good, if it lies between 1 and 1.4 the model was poor, and if it is < 1 the model does not qualify application (Gaston et al., 2010). Similarly, the error range rate (RER) is the ratio between calibration interval and SEP. If RER>10 then the model has good prediction accuracy (Brasil, Cruz-Tirado, & Barbin, 2022). The maximum R^2 value and minimum SE and bias values of a model indicate its good prediction accuracy.

$$R^2 = \frac{\left[\sum\left(Y_p - \overline{Y_P}\right)\left(Y_o - \overline{Y_o}\right)\right]^2}{\sum\left(Y_p - \overline{Y_P}\right)^2\left(Y_o - \overline{Y_o}\right)^2} \quad (1)$$

$$SE = \frac{SD}{\sqrt{n}} \quad (2)$$

$$SD = \sqrt{\frac{\sum_{i=1}^{N}(x_i - \bar{x})^2}{n-1}} \quad (3)$$

$$Bias = \frac{\sum\left(Y_o - Y_p\right)}{n} \quad (4)$$

$$RPD_{CV} = \frac{SD}{SE_{CV}} \quad (5)$$

$$RER = \frac{Range}{SEP} \quad (6)$$

Where Y_O and Y_P are actual and predicted values, respectively, SD is standard deviation and n is number of samples.

Fisher's F test was adopted in order to test the statistical significance (P = 0.05) between the statistical results (SE_{CV} and RPD_{CV}) of PLSR model constructed with raw and pre-processed spectral data (Mahanti et al., 2020). The following equation was used to calculate the F value

$$F = \frac{(SE_{CV_2})^2}{(SE_{CV_1})^2} \quad (7)$$

where, SE_{CV1} and SE_{CV2} are standard error (cross-validation) of two different models developed using raw and pre-processed data, respectively, and SE_{CV2}>SE_{CV1}. The $F_{critical}$ (1-P, n_2-1, n_1-1) read from F table at P = 0.05 and n-1 degree of freedom will be compared with the F value. If $F_{critical}$ is lower than the F value then there is a significant difference between the two SE_{CV}.

2.7. Partial least square discriminant analysis (PLS-DA)

PLS-DA is the combination of regression power of partial least square (PLS) and discrimination power of discriminate analysis. It is a linear supervised classification technique. This classification technique was adopted for the classification of DSC as per the level of adulteration (0, 10, 20, 30, 40, 50, 60, 70, 80, 90 and 100%). The optimum number of latent variables (LVs) were choosen based on the lowest root mean square error (RMSE) obtained during model cross-validation, after which the addition of new LV does not improve model performance significantly (Cruz-Tirado et al., 2021). The Venetian blind cross-validation approach with five groups was adopted for model cross-validation. The performance of PLS-DA model was evaluated based on the classification measures such as sensitivity, specificity, error-rate and accuracy

$$Sensitivity = \frac{TP}{TP + FN} \quad (8)$$

$$Specificity = \frac{TN}{FP + TN} \quad (9)$$

$$Errorrate = 1 - \left(\frac{Sensitivity + Specificity}{2}\right) \quad (10)$$

$$Precision = \frac{TP}{FP + FP} \quad (11)$$

where, TP = true positive; TN = true negative; FP = false positive and FN-false negative (Brasil et al., 2022; Cruz-Tirado et al., 2021).

3. Results and discussion

3.1. Spectral signature

The spectral signature of DCP at different levels of adulteration exhibited a similar pattern irrespective of the level of adulteration (Fig. 1). The coconut powder consists of different biochemical

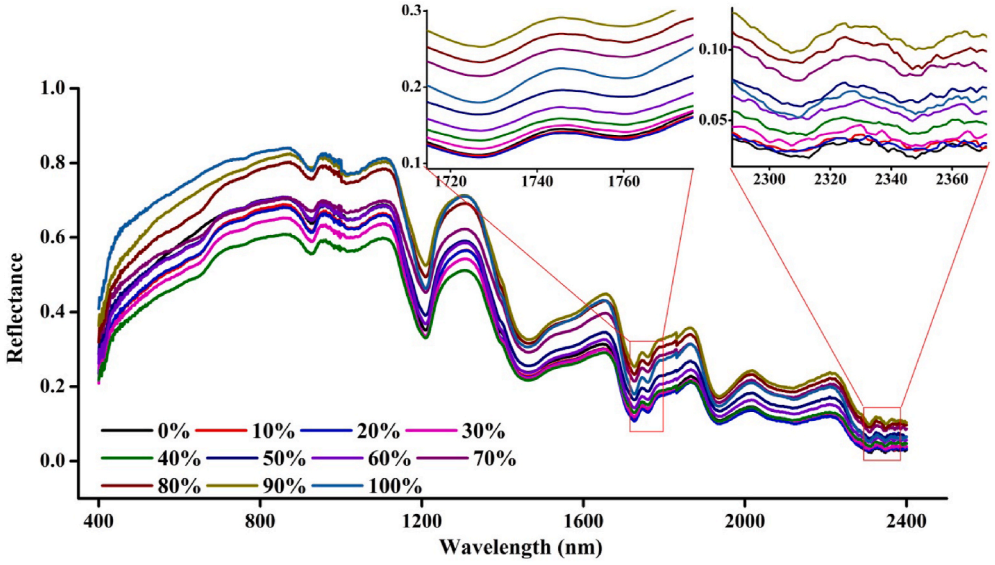

Fig. 1. Spectral signature of desiccated coconut powder adulterated with different levels of coconut milk residue.

compounds such as carbohydrates, fat, protein, water, fiber, etc., which are responsible for the spectral absorption features (Manikantan et al., 2015; Siriphanich et al., 2011). The scatter in reflectance data could be attributed to the variation in particle size besides the chemical composition of the samples. The reflectance values of samples decreased with an increase in the level of adulteration from 0 to 50% however, beyond that the reflectance values increased with an increase in the level of adulteration (60–100%). This might be due to the variation in particle size between DSC and CMR. The increase in level of adulteration causes a rise in the proportion of small particle sizes (CMR) in the sample, as a result of that the reflectance values increases with an increase in adulteration following a specified threshold (50% adulteration). Previous studies have also reported the phenomenon of increase in the reflectance values following a decrease in particle size of sugar (Brauer et al., 2015) and ammonium chloride (Su et al., 2014).

The lower reflectance values of coconut powder were observed at a spectral range (400 nm) thereafter the reflectance values were found to increase and reached a peak at 830 nm. The dips in reflectance values were observed at 927 nm and 1206 nm are indicative of the C–H stretching vibration of $–CH_2$ or $–CH_3$ which are associated with the fat or fatty acids (C–H 3_{rd} and 2_{nd} over tone stretching) (Dixit et al., 2017; Downey et al., 2002). However, small peaks around 944 nm and 1450 nm were identified could be attributed to O–H second and first stretching overtones, respectively and are correlated with the water molecules present in the coconut powder (Dixit et al., 2017). Bands around 1200 nm arise from 2^{nd} overtones of C–H stretching modes of the CH_3 and CH_2 groups (Downey et al., 2002; Kasemsumran et al., 2005). The spectral band at 1400–1550 nm was associated with the vibrations of O–H, C–H, and N–H groups. Similarly, the spectral band between 1650 and 1800 nm was ascribed to the vibration of C–H, C═O, and water O–H groups (Sanaeifar et al., 2020). Tiny troughs at 1728 nm, and 1766 nm arise due to the 1^{st} and 2^{nd} overtones of C–H stretching vibrations of methyl, methylene, ethylene and CH═CH in glycerides (Chen et al., 2018). According to Downey et al. (2002), the absorption at 1725 nm was due to the fatty acid component oleic acid whereas the absorption at 1725 and 1760 nm could be due to the compounds such as saturate and *trans*-unsaturated triglycerides. The variation in spectral reflectance values at this spectral band was due to the inherent differences in fatty acid content between DCP and CMR. The level of fatty acid content varies with the coconut powder composition. A trough around 1930 nm was associated with the O–H stretching and O–H deformation which is related to water content (Morsy & Sun, 2013). The spectral band between 2100and 2200 nm was dominated by the vibration of N–H bending and C═O stretching (Sanaeifar et al., 2020). The small trough at 2125 nm was attributed to the presence of cis double bonds (Downey et al., 2002). The small dips around 2312 nm and 2343 nm arise due to the C–H stretching vibrations and C–H bending and other vibrational modes (Downey et al., 2002; Pu et al., 2008). The combination bands arising from C–H stretching overtones at 2136, and 2346 nm are related to fat or fatty acid content (Dixit et al., 2017). The reflectance values of coconut powder decreased with an increase in level of adulteration from 0 to 40%, but the reflectance values of desiccated coconut powder increased with an increase in level of adulteration between 50 and 100% within the spectral range of 400–1300 nm.

3.2. Principal component analysis (PCA)

The raw spectral data were mean centered prior to performing PCA. The first two principal components were selected as optimum since the components explained 97.56% of product variance. The variances explained by the 1^{st} and 2^{nd} PC were 89.48 and 8.08%, respectively. The score plot between PC1 and PC2 for all the samples is shown in Fig. 2a. From this figure, it is evident that the samples were grouped based on the concentration of adulterant. A clear distinction of low and high adulteration levels was observed, but on the other hand, no clear distinction among the successive adulteration levels was observed. As spectroscopy is a point scan technique which collects average spectral data within its field of view (FOV) and hence it did not consider the spatial variation. Therefore, during sampling uneven distribution/absence of adulterant within the sampling area causes a spectral deviation when compared with the true sample. In PC1 the samples which has adulterant level between 0 and 40% exhibited negative scores, whereas the samples which have adulterant concentration between 50 and 60% falls on the both negative and positive quadrants and samples whose adulteration level more than 60% showed positive scores. Therefore, it can be stated that PC1 reflects the level of adulteration in DCP. On the other hand, PC2 represents the product characteristics. The peaks were observed at 653, 930, 1039, 1180, 1210, 1238, 1316, 1360, 1650, 1728, 1872 and 1924 nm (Fig. 2b). These wavelengths are responsible for the chemical constituents present in both the coconut powders.

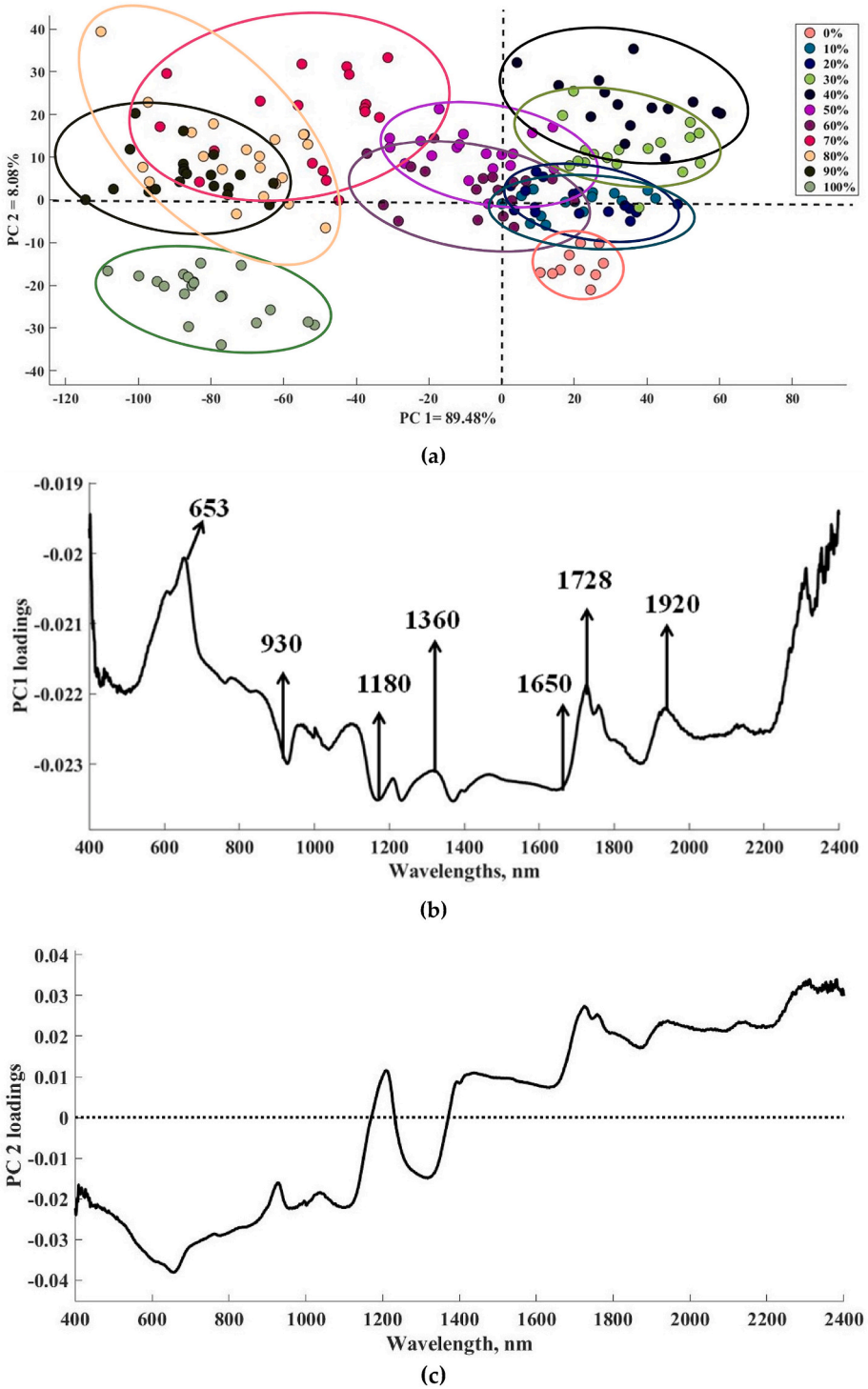

Fig. 2. Principal component analysis of spectral data of DSC adulterated with CMR at different levels, (a) score plot between PC1 and PC2; (b) PC1 loading plot and (c) PC2 loading plot.

3.3. PLSR model

3.3.1. PLSR model based on full spectral data

The spectral data at the beginning and end of the spectrum suffers from low signal to noise ratio therefore the spectral data at the beginning 350–400 nm and at the end 2400–2500 nm were excluded for the model development. The PLSR model was developed using raw and pre-processed spectral data (400–2400 nm). The optimum latent variables (LVs) were selected based on the explained variance, where no further increase in explained variance was observed during model calibration and cross-validation. The assortment of LVs more than the optimum LVs results in model over-fitting as a result of it the RMSE during CV increases and during C decreases.

The slope, R^2, SE, bias and RPD value of developed models during calibration and cross-validation varied between 0.820-0.930, 0.950–0.980, 8.320–13.220, −0.201–0.083 and 9.381–11.489, respectively according to the pre-processing techniques. The performance of PLSR model developed using a raw spectral data delivers a good

prediction accuracy ($R^2_P = 0.973$; $SE_P = 9.681$; $RPD_P = 9.381$; $RER_P = 10.389$) over other pre-processing techniques (Table 1). In accordance with this observation, previous studies have reported that the performance of PLSR models developed using the raw spectral data yields appreciable results over the pre-processed spectral data (Yu et al., 2018; Zhao et al., 2016).

The RPD values of all the models were higher than the 2.5, implying that the model has an excellent prediction accuracy (Mahanti et al., 2020). The statistical results obtained during model calibration, cross validation and prediction are close to each other, suggesting that the developed model was free from over and under fitting. The RER values of all the models developed with full spectral data were higher than the 10 this implies the developed models have good prediction capacity. For some of the samples having an adulteration level of <10%, the model predicted negative values (Fig. 3). The pre-processing of spectral data did not have a significant effect on the model performance (Table 1). Therefore, the model developed using the raw spectral data was selected as the best and was used further for the selection of variables.

3.3.2. PLSR model with selected variables

The performance of PLSR model developed using the raw spectral data was better than the models developed with pre-processed spectral data; therefore, it was selected for the variable selection. The significant wavelengths were selected from the plot between regression coefficients and wavelengths (Fig. 4a). The significant wavelengths which have high regression coefficients (i.e 653, 933, 1189, 1383, 1444, 1670, and 1911 nm), irrespective of its sign, were selected. The wavelength 653 nm corresponds to the brown colour testa present in the coconut milk residue. In general, while preparing DCP the testa portion is removed but whole coconut copra along with testa was also used while preparing CMR (Manikantan et al., 2018). The wavelength 933 nm corresponds to C–H 3rd stretching overtone which is related to the fat/fatty acids present in the coconut powder (Dixit et al., 2017). The wavelength 1189 nm was responsible for the N–H bond as a result of protein content in the coconut powder (Morsy & Sun, 2013). However, the wavelength 1383 nm represents C–H bonds of lipids present in coconut powder (Sato, 2008). The wavelength 1444 nm was associated with the C–H stretching and C–H deformation represents the fat content (Bian et al., 2013). The wavelength 1670 nm is associated with the N–H overtone related to the protein content of coconut powder (Morsy & Sun, 2013). Similarly, the wavelength 1911 nm corresponds to the O–H bend 2nd overtones, which is related to water present in the coconut powder (Dixit et al., 2017; Sanaeifar et al., 2020). The PLSR model was developed using these selected wavelengths with an optimum LVs equal to five. The statistical results obtained during model calibration ($R^2_C = 0.973$; $SE_C = 9.672$; $RPD_C = 11.489$) (Fig. 4b), cross-validation ($R^2_{CV} = 0.971$; $SE_{CV} = 10.019$; $RPD_{CV} = 11.297$) (Fig. 4c) and prediction ($R^2_P = 0.961$; $SE_P = 11.701$; $RPD_P = 9.381$) (Fig. 4d) are close to each other suggesting the model is free from the over and under fitting. The RPD values of the model developed during calibration, cross-validation, and prediction was greater than 2.5 suggesting the performance of the model was excellent (Gaston et al., 2010). No significant difference in statistical results was observed between the model developed using the raw whole spectral data ($R^2_P = 0.973$; $SE_P = 9.681$; $RPD_P = 9.381$; $RER_P = 10.389$) and model developed using the selected wavelengths ($R^2_P = 0.869$; $SE_P = 11.701$; $RPD_P = 9.381$; $RER_P = 8.595$). The latter model was superior over the former because the number of variables showed a drastic decline from 2001 to seven. As a result of it, the computational load and complexity decreases and the computational power of the model increases. However, in the case of PLSR model developed using full spectral data, some of the samples were predicted with negative values which was not observed in model developed with selected wavelengths.

3.4. PLS-DA

The adulterated DSC powders were classified based on the level of adulteration using PLS-DA technique. The optimum number of LVs were selected as two based on the error-rate. The first two LVs explained more than 98% of total product variance as LV1 explained 91.5% of variance, and LV2 could explain 6.57% of variance. The first LV could separate the DSC samples based on the level of adulteration. The second LVs could explain the product composition and size of the DSC and CMR. The confusion matrix generated during model calibration (Fig. 5a), cross-validation (Fig. 5b) and prediction (Fig. 5c) is depicted in Fig. 5. From these confusion matrices, it is revealed that the samples were assigned to their respective classes suitably based on the level of adulteration both at low (0–30%) and high level (70–100%) of adulteration (Fig. 5). However, samples that have adulteration levels ranging from 40 to 60% were misclassified and were assigned to the neighbor classes (Fig. 5). This could be due to the absence/presence of adulterant or appreciably high or low concentration of adulterant than the targeted adulteration at the point of scan while data acquisition, because of the accumulation of sample at the bottom layers of Petri dishes. The classification measures such as sensitivity, specificity and precision of each class were tabulated in Table 2.

The sensitivity of classes from 40 to 80% was lower (<0.5) whereas for the remaining classes it was higher (>0.88). Even though the sensitivity was low for most of these classes the samples were assigned to successive classes only (minimum error). The specificity for all the classes was higher than the 0.9. The precision for classes 10, 20, 40, 50, 70 and 80% was <70%, attributable to the wrong assignment of samples in the neighboring classes. But most of the samples are assigned to the neighboring classes (less error) except for the samples having 50 and 60% level of adulteration. This error may because due to the uneven

Table 1
The statistical results of PLSR model developed with raw and pre-processed spectral data for estimation of level of adulteration in desiccated coconut powder (DCP).

Pre-processing technique		LVs	Slope	R^2	RMSE	SE	bias	RPD	RER	$F_{critical}$
Raw	C	5	0.930	0.980	8.289	8.320	0.023	11.489		1.334
	CV	5	0.921	0.977	8.929	8.963	−0.005	11.489		1.334
	P	5	0.909	0.973	9.626	9.681	−0.039	9.381	10.389	1.426
MSC + SNV	C	5	0.916	0.976	9.141	9.176	−0.001	11.489		1.334
	CV	5	0.904	0.971	10.080	10.118	0.054	11.489		1.334
	P	5	0.902	0.972	9.884	9.941	−0.003	9.381	10.117	1.426
SG smoothing	C	3	0.899	0.971	10.129	10.167	−0.031	11.489		1.334
	CV	3	0.820	0.950	13.172	13.220*	−0.201	11.489		1.334
	P	3	0.917	0.976	9.104	9.156	−0.004	9.381	10.984	1.426
Detrending	C	4	0.924	0.980	8.458	8.489	0.083	11.489		1.334
	CV	4	0.914	0.975	9.292	9.327	0.073	11.489		1.334
	P	4	0.898	0.971	9.994	10.051	0.033	9.381	10.006	1.426
Selected wavelengths	C	5	0.909	0.973	9.635	9.672	−0.048	11.489		1.334
	CV	5	0.906	0.971	9.981	10.019	−0.118	11.297		1.334
	P	5	0.869	0.961	11.635	11.701	−0.095	9.381	8.595	1.426

C-calibration; CV-Cross validation; P-Prediction; MSC-Multiplicate scatter correction; SNV-Standard normal variate; SG-Savitzky–Golay.; RER- Error range rate.

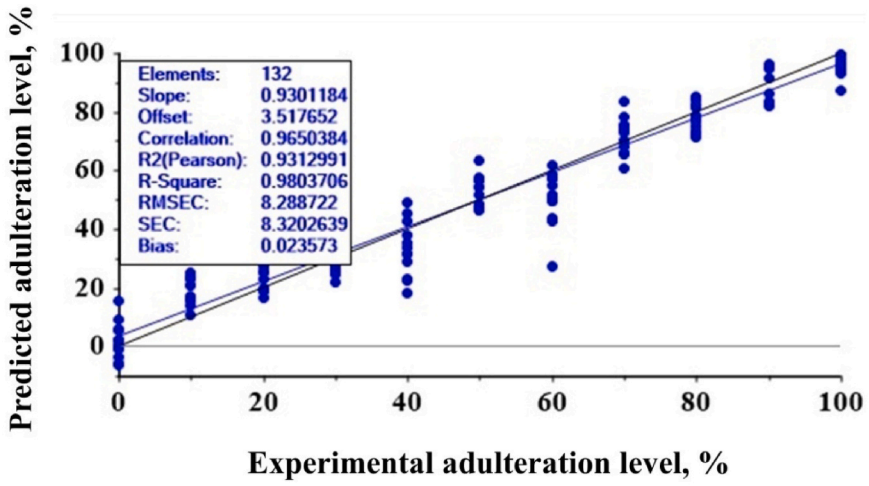

(a)

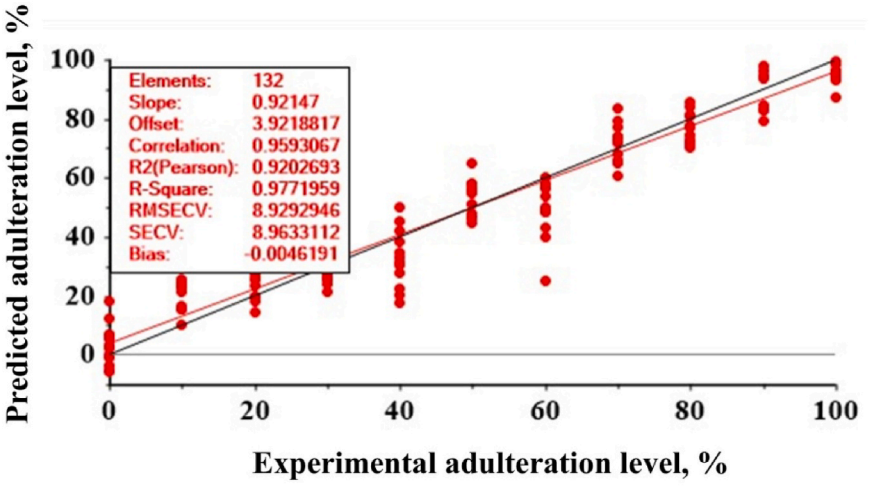

(b)

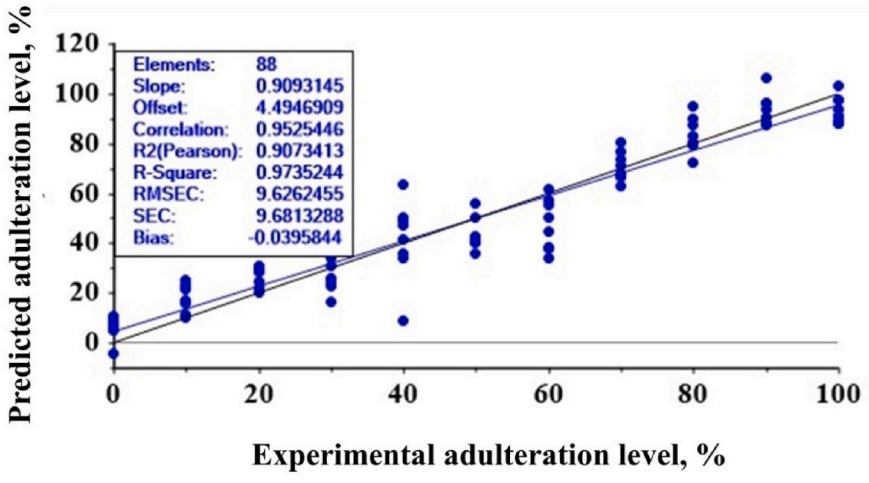

(c)

Fig. 3. PLSR model developed with raw spectral data actual and predicted level of desiccated coconut powder adulteration (a) calibration; (b) cross validation and (c) prediction.

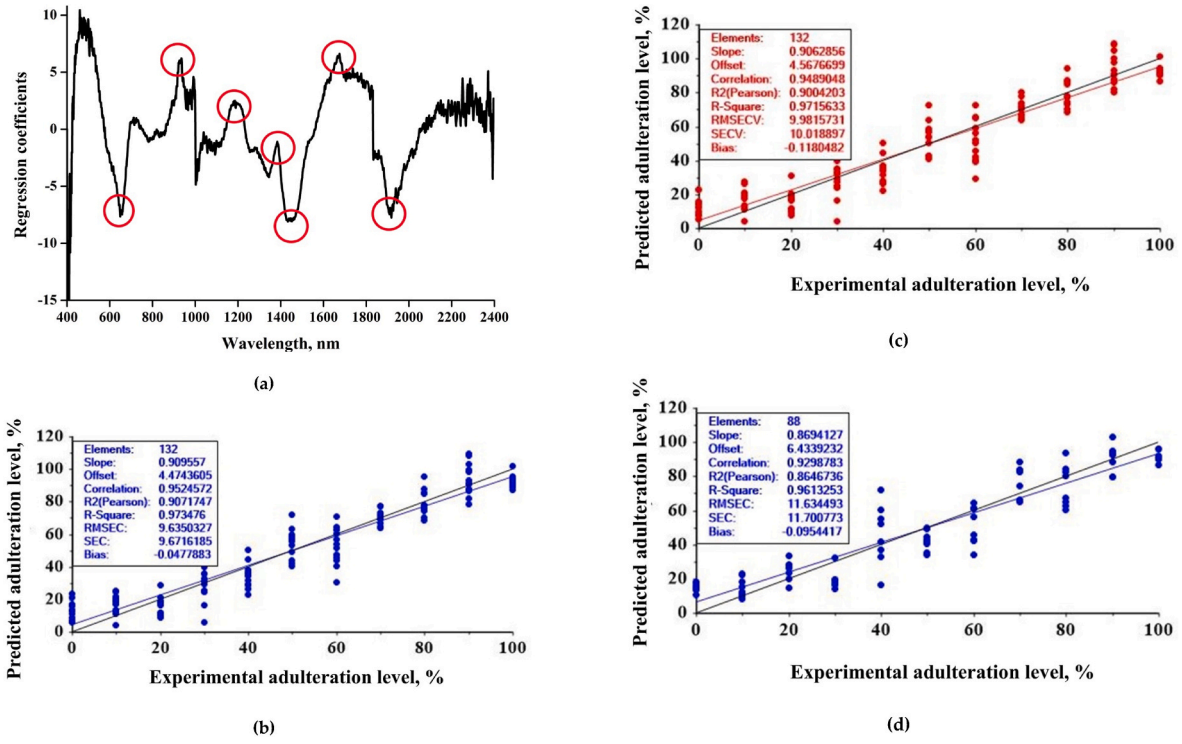

Fig. 4. PLSR model using selected wavelengths (a) selection of featured wavelengths; actual *vs* predicted adulteration level (b) calibration; (c) cross-validation and (d) prediction.

Predicted class / True class

Class	0	10	20	30	40	50	60	70	80	90	100
0	10	0	2	0	0	0	0	0	0	0	0
10	0	8	3	0	0	0	1	0	0	0	0
20	0	1	10	1	0	0	0	0	0	0	0
30	1	0	1	10	0	0	0	0	0	0	0
40	0	0	1	1	9	0	0	1	0	0	0
50	0	0	0	0	0	10	2	0	0	0	0
60	0	1	1	0	0	2	8	0	0	0	0
70	0	0	0	0	0	0	0	12	0	0	0
80	0	0	0	0	0	0	1	0	11	0	0
90	0	0	0	0	0	0	0	0	0	12	0
100	0	0	0	0	0	0	0	0	0	0	12

(a)

Predicted class / True class

Class	0	10	20	30	40	50	60	70	80	90	100
0	10	1	0	1	0	0	0	0	0	0	0
10	0	6	4	1	0	0	1	0	0	0	0
20	0	3	7	2	0	0	0	0	0	0	0
30	1	0	0	10	0	0	1	0	0	0	0
40	0	0	1	1	9	0	0	1	0	0	0
50	0	0	0	0	1	8	3	0	0	0	0
60	0	1	1	1	0	3	6	0	0	0	0
70	0	0	0	0	1	0	0	11	0	0	0
80	0	0	0	0	0	0	1	0	11	0	0
90	0	0	0	0	0	0	0	0	0	12	0
100	0	0	0	0	0	0	0	0	0	0	12

(b)

Predicted class / True class

Class	0	10	20	30	40	50	60	70	80	90	100
0	7	0	0	0	0	1	0	0	0	0	0
10	0	7	1	0	0	0	0	0	0	0	0
20	0	1	7	0	0	0	0	0	0	0	0
30	0	0	1	7	0	0	0	0	0	0	0
40	0	2	0	2	3	1	0	0	0	0	0
50	0	0	2	1	2	3	0	0	0	0	0
60	0	3	0	0	1	0	4	0	0	0	0
70	0	0	0	0	0	0	1	4	3	0	0
80	0	0	0	0	0	0	0	3	4	1	0
90	0	0	0	0	0	0	0	0	0	8	0
100	0	0	0	0	0	0	0	0	0	0	8

(c)

Fig. 5. Confusion matrix of PLS-DA technique during model (a) calibration; (b) cross-validation and (c) prediction.

distribution or accumulation of adulterants at the bottom of Petri plates during the process of data acquisition. On the other hand, the difference in particle size between DSC and CMR causes variation in magnitude of reflectance values (Fig. 1) resulting in some of the samples being wrongly assigned to neighboring classes. The classification accuracy reported by previous studies for evaluation of egg freshness (Brasil et al.,

Table 2
Classification measures of PLS-DA technique.

	Calibration			Cross-Validation			Prediction		
Class	Sensitivity	Specificity	Precision	Sensitivity	Specificity	Precision	Sensitivity	Specificity	Precision
0	0.83	0.99	0.91	0.83	0.99	0.91	0.88	1.00	1.00
10	0.67	0.98	0.80	0.50	0.96	0.55	0.88	0.93	0.54
20	0.83	0.93	0.56	0.58	0.95	0.54	0.88	0.95	0.64
30	0.83	0.98	0.83	0.83	0.95	0.63	0.88	0.96	0.70
40	0.75	1.00	1.00	0.75	0.98	0.82	0.38	0.96	0.50
50	0.83	0.98	0.83	0.67	0.97	0.73	0.38	0.97	0.60
60	0.67	0.97	0.67	0.50	0.95	0.50	0.50	0.99	0.80
70	1.00	0.99	0.92	0.92	0.99	0.92	0.50	0.96	0.57
80	0.92	1.00	1.00	0.92	1.00	1.00	0.50	0.96	0.57
90	1.00	1.00	1.00	1.00	1.00	1.00	1.00	0.99	0.89
100	1.00	1.00	1.00	1.00	1.00	1.00	1.00	1.00	1.00

2022; Cruz-Tirado et al., 2021) and discrimination of naturally and artificially ripened sapota (Mahanti & Chakraborty, 2020) was higher than the present study. PLS-DA is a linear classification technique, the classification power in the present study was relatively less because of the high number of classes (11 classes) examined herein compared to the previous studies (2 classes).

4. Conclusions

The adulteration level of desiccated coconut powder with coconut residue could be estimated effectively with the help of spectral reflectance data along with PLSR model. The PLSR model developed with raw spectral data has greater predictive capacity and robustness. This model has capablility to predict the level of adulteration with standard error < 10%. The predictive capability of PLSR model developed with selected wavelengths (653, 933, 1189, 1383, 1444, 1670, and 1911 nm) was significantly identical to the model constructed with whole spectral data. However, the computational load and complexity of the model decreased and the computational power of model developed with selected wavelengths increased due to decrease in the number of variables (wavelengths). The PLS-DA technique depicted average classification accuracy of more than 70%. The results obtained in the present study affirm that the vis-NIR spectroscopy along with the suitable chemometric techniques is an effective tool for rapid detection of adulteration in DCP.

Declaration of competing interest

None.

Declaration of competing interest

The authors declare that they have no conflict of interest.

CRediT authorship contribution statement

R. Pandiselvam: Conceptualization, Investigation, Methodology, Validation, Writing – original draft. **Naveen Kumar Mahanti:** Methodology, Data curation, Validation, Writing – original draft. **M.R. Manikantan:** Methodology, Validation, Formal analysis, Draft editing, Supervision. **Anjineyulu Kothakota:** Methodology, Validation, Formal analysis, Draft editing, Supervision. **Subir Kumar Chakraborty:** Validation, Formal analysis. **S.V. Ramesh:** Formal analysis, Resources, Writing – original draft. **P.P. Shameena Beegum:** Formal analysis, Resources, Writing – original draft.

Acknowledgements

Authors are grateful to AICRP on PHET (Indian Council of Agricultural Research), Ludhiana, India for financial support. Authors wish to thank the Director, ICAR-Central Institute of Agricultural Engineering, Bhopal for providing necessary facilities to conducting the experiment.

References

Arjun, A. D., Chakraborty, S. K., Mahanti, N. K., & Kotwaliwale, N. (2021). Non-destructive assessment of quality parameters of white button mushrooms (Agaricus bisporus) using image processing techniques. *Journal of Food Science & Technology*, 1–13.

ASABE. (2003). *ASABE Standards S319.3. Method of determining and expressing fineness of feed materials by sieving.* St. Joseph, MI, USA.

Barbin, D., Elmasry, G., Sun, D. W., & Allen, P. (2012). Near-infrared hyperspectral imaging for grading and classification of pork. *Meat Science, 90*(1), 259–268. https://doi.org/10.1016/j.meatsci.2011.07.011

Bian, M., Skidmore, A. K., Schlerf, M., Wang, T., Liu, Y., Zeng, R., & Fei, T. (2013). Predicting foliar biochemistry of tea (Camellia sinensis) using reflectance spectra measured at powder, leaf and canopy levels. *ISPRS Journal of Photogrammetry and Remote Sensing, 78*, 148–156. https://doi.org/10.1016/j.isprsjprs.2013.02.002

Brasil, Y. L., Cruz-Tirado, J. P., & Barbin, D. F. (2022). Fast online estimation of quail eggs freshness using portable NIR spectrometer and machine learning. *Food Control, 131*, 108418. https://doi.org/10.1016/j.foodcont.2021.108418

Brauer, C. S., Johnson, T. J., Myers, T. L., Su, Y.-F., Blake, T. A., & Forland, B. M. (2015). Effects of sample preparation on the infrared reflectance spectra of powders. *Chemical, Biological, Radiological, Nuclear, and Explosives (CBRNE) Sensing XVI*. https://doi.org/10.1117/12.2179736

Chakraborty, S. K., Mahanti, N. K., Mansoori, S. M., Tripathi, M. K., Kotwaliwale, N., & Jayas, D. S. (2021). Non-destructive classification and prediction of aflatoxin-B1 concentration in maize kernels using Vis-NIR (400-1000 nm) hyperspectral imaging. *Journal of Food Science & Technology, 58*, 437–450. https://doi.org/10.1007/s13197-020-04552-w

Chen, H., Lin, Z., & Tan, C. (2018). Fast quantitative detection of sesame oil adulteration by near-infrared spectroscopy and chemometric models. *Vibrational Spectroscopy, 99*, 178–183. https://doi.org/10.1016/j.vibspec.2018.10.003

Coconut Development Board. (2017). Desiccated coconut-the profile. *Indian Coconut Journal, 7*, 9–11.

Correia, R. M., Tosato, F., Domingos, E., Rodrigues, R. R. T., Aquino, L. F. M., Filgueiras, P. R., Lacerda, V., & Romão, W. (2018). Portable near infrared spectroscopy applied to quality control of Brazilian coffee. *Talanta, 176*, 59–68. https://doi.org/10.1016/j.talanta.2017.08.009

Cruz-Tirado, J. P., da Silva Medeiros, M. L., & Barbin, D. F. (2021). On-line monitoring of egg freshness using a portable NIR spectrometer in tandem with machine learning. *Journal of Food Engineering, 306*, 110643. https://doi.org/10.1016/j.jfoodeng.2021.110643

DebMandal, M., & Mandal, S. (2011). Coconut (*Cocos nucifera* L.: Arecaceae): In health promotion and disease prevention. *Asian Pacific journal of tropical medicine, 4*(3), 241–247.

Dixit, Y., Casado-Gavalda, M. P., Cama-Moncunill, R., Cama-Moncunill, X., Markiewicz-Keszycka, M., Cullen, P. J., & Sullivan, C. (2017). Developments and challenges in online NIR spectroscopy for meat processing. *Comprehensive Reviews in Food Science and Food Safety, 16*(6), 1172–1187. https://doi.org/10.1111/1541-4337.12295

Downey, G., McIntyre, P., & Davies, A. N. (2002). Detecting and quantifying sunflower oil adulteration in extra virgin olive oils from the Eastern Mediterranean by visible and near-infrared spectroscopy. *Journal of Agricultural and Food Chemistry, 50*(20), 5520–5525. https://doi.org/10.1021/jf0257188

Gaston, E., Frias, J. M., Cullen, P. J., O'Donnell, C. P., & Gowen, A. A. (2010). Prediction of polyphenol oxidase activity using visible nearinfrared hyperspectral imaging on mushroom (Agaricus bisporus) caps. *Journal of Agricultural and Food Chemistry, 58*, 6226–6233. https://doi.org/10.1021/jf100501q

Giraudo, A., Grassi, S., Savorani, F., Gavoci, G., Casiraghi, E., & Geobaldo, F. (2019). Determination of the geographical origin of green coffee beans using NIR spectroscopy and multivariate data analysis. *Food Control, 99*, 137–145. https://doi.org/10.1016/j.foodcont.2018.12.033

Guelpa, A., Marini, F., du Plessis, A., Slabbert, R., & Manley, M. (2017). Verification of authenticity and fraud detection in South African honey using NIR spectroscopy. *Food Control, 73*, 1388–1396. https://doi.org/10.1016/j.foodcont.2016.11.002

Iqbal, A., Sun, D. W., & Allen, P. (2013). Prediction of moisture, color and pH in cooked, pre-sliced Turkey hams by NIR hyperspectral imaging system. *Journal of Food Engineering, 117*(1), 42–51. https://doi.org/10.1016/j.jfoodeng.2013.02.001

Jiménez-Carvelo, A. M., Lozano, V. A., & Olivieri, A. C. (2019). Comparative chemometric analysis of fluorescence and near infrared spectroscopies for authenticity confirmation and geographical origin of Argentinean extra virgin olive oils. *Food Control, 96*, 22–28. https://doi.org/10.1016/j.foodcont.2018.08.024

Kaczmarczyk, M. M., Miller, M. J., & Freund, G. G. (2012). The health benefits of dietary fiber: Beyond the usual suspects of type 2 diabetes mellitus, cardiovascular disease and colon cancer. *Metabolism Clinical and Experimental, 61*(8), 1058–1066. https://doi.org/10.1016/j.metabol.2012.01.017. PMid:22401879.

Kasemsumran, S., Kang, N., Christy, A., & Ozaki, Y. (2005). Partial least squares processing of near-infrared spectra for discrimination and quantification of adulterated olive oils. *Spectroscopy Letters, 38*(6), 839–851. https://doi.org/10.1080/00387010500316189

Khuwijitjaru, P., Watsanit, K., & Adachi, S. (2012). Carbohydrate content and composition of product from subcritical water treatment of coconut meal. *Journal of Industrial and Engineering Chemistry, 18*(1), 225–229. https://doi.org/10.1016/j.jiec.2011.11.010

Mahanti, N. K., & Chakraborty, S. K. (2020). Application of chemometrics to identify artificial ripening in sapota (Manilkara Zapota) using visible near infrared absorbance spectra. *Computers and Electronics in Agriculture, 175*, 105539. https://doi.org/10.1016/j.compag.2020.105539

Mahanti, N. K., Chakraborty, S. K., Kotwaliwale, N., & Vishwakarma, A. K. (2020). Chemometric strategies for non-destructive and rapid assessment of nitrate content in harvested spinach using Vis-NIR spectroscopy. *Journal of Food Science, 85*(10), 3653–3662. https://doi.org/10.1111/1750-3841.15420

Manaf, M. A., Man, Y. B. C., Hamid, N. S. A., Ismail, A., & Abidin, S. Z. (2007). Analysis of adulteration of virgin coconut oil by palm kernel olein using Fourier transform infrared spectroscopy. *Journal of Food Lipids, 14*(2), 111–121. https://doi.org/10.1111/j.1745-4522.2007.00066.x

Manikantan, M. R., Ambrose, R. P. K., & Alavi, S. (2015). Flow-specific physical properties of coconut flours. *International Agrophysics, 29*(4). https://doi.org/10.1515/intag-2015-0051

Manikantan, M. R., Pandiselvam, R., Beegum, S., & Mathew, A. C. (2018). Harvest and postharvest technology. In *The coconut palm (Cocos nucifera L.)-Research and Development perspectives* (pp. 635–722). Singapore: Springer. https://doi.org/10.1007/978-981-13-2754-4_13.

Mansor, T. S. T., Man, Y. B. C., & Rohman, A. (2011). Application of fast gas chromatography and Fourier transform infrared spectroscopy for analysis of lard adulteration in virgin coconut oil. *Food Analytical Methods, 4*(3), 365–372. https://doi.org/10.1007/s12161-010-9176-y

Morsy, N., & Sun, D. W. (2013). Robust linear and non-linear models of NIR spectroscopy for detection and quantification of adulterants in fresh and frozen-thawed minced beef. *Meat Science, 93*, 292–302. https://doi.org/10.1016/j.meatsci.2012.09.005

Pandiselvam, R., Manikantan, M. R., Sunoj, S., Sreejith, S., & Beegum, S. (2019). Modeling of coconut milk residue incorporated rice-corn extrudates properties using multiple linear regression and artificial neural network. *Journal of Food Process Engineering, 42*(2), Article e12981. https://doi.org/10.1111/jfpe.12981

Park, B., Abbott, J. A., Lee, K. J., Choi, C. H., & Choi, K. H. (2003). Near-infrared diffuse reflectance for quantitative and qualitative measurement of soluble solids and firmness of delicious and gala apples. *Transactions of the American Society of Agricultural Engineers, 46*, 1721–1731. https://doi.org/10.13031/2013.15628

Park, Y., Subar, A. F., Hollenbeck, A., & Schatzkin, A. (2011). Dietary fiber intake and mortality in the NIH-AARP diet and health study. *Archives of Internal Medicine, 171*(12), 1061–1068. https://doi.org/10.1001/archinternmed.2011.18. PMid:21321288.

Picouet, P. A., Gou, P., Hyypiö, R., & Castellari, M. (2018). Implementation of NIR technology for at-line rapid detection of sunflower oil adulterated with mineral oil. *Journal of Food Engineering, 230*, 18–27. https://doi.org/10.1016/j.jfoodeng.2018.01.011

Pu, Y., Ragauskas, A. J., Lucia, L. A., Naithani, V., & Jameel, H. (2008). Near-infrared spectroscopy and chemometric analysis for determining oxygen delignification yield. *Journal of Wood Chemistry and Technology, 28*(2), 122–136.

Ravikanth, L., Jayas, D. S., White, N. D. G., Fields, P. G., & Sun, D. W. (2017). Extraction of spectral information from hyperspectral data and application of hyperspectral imaging for food and agricultural products. *Food and Bioprocess Technology, 10*(1), 1–33. https://doi.org/10.1007/s11947-016-1817-8

Romero, I. (2010). PCA-based noise reduction in ambulatory ECG's. *Computers in Cardiology*, 677–680.

Roy, K., Kar, S., & Das, R. N. (2015). Selected statistical methods in QSAR, 1st edition, chapter-6. In K. Roy, S. Kar, & R. N. Das (Eds.), *Understanding the basics of QSAR for applications in pharmaceutical sciences and risk assessment* (pp. 191–228). Cambridge, Massachusetts: United States of America. https://doi.org/10.1016/C2014-0-00286-9.

Sanaeifar, A., Huang, X., Chen, M., Zhao, Z., Ji, Y., Li, X., He, Y., Zhu, Y., Chen, X., & Yu, X. (2020). Nondestructive monitoring of polyphenols and caffeine during green tea processing using Vis-NIR spectroscopy. *Food Sciences and Nutrition, 8*(11), 5860–5874. https://doi.org/10.1002/fsn3.1861

Sato, T. (2008). Nondestructive measurements of lipid content and fatty acid composition in rapeseeds (Brassica napus L.) by near infrared spectroscopy. *Plant Production Science, 11*(1), 146–150. https://doi.org/10.1626/pps.11.146

Sebastian, K. S. (2017). Quantum leap in desiccated coconut powder export. *Indian Coconut Journal, 6*, 4–6.

Shao, Y., Xuan, G., Hu, Z., & Gao, X. (2018). Identification of adulterated cooked millet flour with Hyperspectral Imaging Analysis. *IFAC-PapersOnLine, 51*, 96–101. https://doi.org/10.1016/j.ifacol.2018.08.068

Siriphanich, J., Saradhuldhat, P., Romphophak, T., Krisanapook, K., Pathaveerat, S., & Tongchitpakdee, S. (2011). Coconut (cocos nucifera L.). In *Postharvest biology and technology of tropical and subtropical Fruits* (pp. 8–35). Woodhead Publishing.

Su, Y.-F., Myers, T. L., Brauer, C. S., Blake, T. A., Forland, B. M., Szecsody, J. E., & Johnson, T. J. (2014). *Infrared reflectance spectra: Effects of particle size, provenance and preparation. Optics and photonics for counterterrorism, crime fighting, and defence X; and optical materials and biomaterials in security and defence systems technology XI*. https://doi.org/10.1117/12.2069954

Su, W.-H., & Sun, D.-W. (2017). Evaluation of spectral imaging for inspection of adulterants in terms of common wheat flour, cassava flour and corn flour in organic Avatar wheat (Triticum spp.) flour. *Journal of Food Engineering, 200*, 59–69. https://doi.org/10.1016/j.jfoodeng.2016.12.014

Trinidad, T. P., Mallillin, A. C., Valdez, D. H., Loyola, A. S., Askali-Mercado, F. C., Castillo, J. C., Encabo, R. R., Masa, D. B., Maglaya, A. S., & Chua, M. T. (2006). Dietary fiber from coconut flour: A functional food. *Innovative Food Science & Emerging Technologies, 7*(4), 309–317. https://doi.org/10.1016/j.ifset.2004.04.003

Xiaobo, Z., Jiewen, Z., Povey, M. J. W., Holmes, M., & Mao, H. (2010). Variable selection methods in near-infrared spectroscopy. *Analytica Chimica Acta, 667*(1–2), 14–32. https://doi.org/10.1016/j.aca.2010.03.048

Yu, X., Lu, H., & Liu, Q. (2018). Deep-learning-based regression model and hyperspectral imaging for rapid detection of nitrogen concentration in oilseed rape (Brassica napus L.) leaf. *Chemometrics and Intelligent Laboratory Systems, 172*, 188–193. https://doi.org/10.1016/j.chemolab.2017.12.010

Zhao, Y. R., Li, X., Yu, K. Q., Cheng, F., & He, Y. (2016). Hyperspectral imaging for determining pigment contents in cucumber leaves in response to angular leaf spot disease. *Scientific Reports, 6*, 27790. https://doi.org/10.1038/srep27790